

RSC Advances



This is an *Accepted Manuscript*, which has been through the Royal Society of Chemistry peer review process and has been accepted for publication.

Accepted Manuscripts are published online shortly after acceptance, before technical editing, formatting and proof reading. Using this free service, authors can make their results available to the community, in citable form, before we publish the edited article. This *Accepted Manuscript* will be replaced by the edited, formatted and paginated article as soon as this is available.

You can find more information about *Accepted Manuscripts* in the [Information for Authors](#).

Please note that technical editing may introduce minor changes to the text and/or graphics, which may alter content. The journal's standard [Terms & Conditions](#) and the [Ethical guidelines](#) still apply. In no event shall the Royal Society of Chemistry be held responsible for any errors or omissions in this *Accepted Manuscript* or any consequences arising from the use of any information it contains.

Cite this: DOI: 10.1039/c0xx00000x

www.rsc.org/xxxxxx

ARTICLE TYPE

Vapour-Liquid-Solid growth of one-dimensional In₂Se₃ nanostructures and its promising field emission behaviour

Sachin R. Suryawanshi,¹ Prashant K. Bankar¹, Mahendra A. More,^{1*} Dattatray J. Late,^{2,*}

Received (in XXX, XXX) Xth XXXXXXXXXX 20XX, Accepted Xth XXXXXXXXXX 20XX

DOI: 10.1039/b000000x

Single crystalline ultra long In₂Se₃ nanowires has been grown employing a single step facile thermal evaporation route under optimized conditions on Au/Si wafers, and morphology dependent field emission investigations on the In₂Se₃ nanostructure at the base pressure $\sim 1 \times 10^{-8}$ mbar are explored. In addition, structural and morphological analysis of as-synthesized In₂Se₃ nanostructures has been carried out using XRD, SEM and TEM. A plausible explanation on the vapor-solid-liquid (VLS) growth mechanism based on the experimental results and reported literature has been presented. Furthermore, field emission measurements demonstrate remarkably enhanced emission behaviour, which is explained on the basis of field enhancement factor and aspect ratio of the nanostructures. The synthesized In₂Se₃ nanowires emitter delivers very high current density of ~ 1.2 mA/cm² at an applied electric field of ~ 6.33 V/ μ m. The present results demonstrate the In₂Se₃ as an important candidate for potential applications in nano/micro-electronic devices.

1. Introduction

Multifunctional one-dimensional (1D) inorganic semiconductor chalcogenides nanostructures such as nanowires, nanobelts and nanoribbons have attracted great interest due to their significance in basic scientific research and potential technological applications.¹⁻⁶ The physico-chemical properties of these inorganic semiconductor chalcogenides can be tailored via shape and size control. Furthermore, they are expected to play important role as both interconnects and the key units of next-generation nanoscale electronic, and optoelectronic devices. Amongst the various chalcogenides, indium selenide (In₂Se₃) is a black crystalline, n- type; A^{III}-B^{VI} group compound with a layered structure. It usually crystallizes into double layers of nonmetal atoms, each consisting of the [Se-In-Se-In-Se] sheets stacked together through the Se atoms along the c-axis. Normally, In₂Se₃ is a direct narrow band gap semiconductor ($E_g \sim 1.35$ eV, at 300 K). The strong intralayer bonding and the weak interlayer van der Waals interactions give rise to highly anisotropic structural, electrical, optical, and mechanical properties, which make the In₂Se₃ an attractive candidate for vacuum micro/nano-electronic devices.⁷⁻¹¹

Recently, various metal chalcogenides, owing to their layered structure and unique set of physico-chemical properties are being re-addressed as graphene analogues. In addition to their potential in various applications including photo detectors, Photocatalytic materials, solar cells (window materials) etc, nanostructures of these materials exhibit promising field electron emission (FE) properties. Our group has investigated FE behaviour of nanostructures of various metal chalcogenides and their nanocomposite like MoS₂, VS₂, WS₂, CdS, GaS, and

WS₂-RGO. In₂Se₃ is one of the important metal chalcogenides and there is no report on the FE studies of In₂Se₃ nanostructures. Furthermore, systematic studies pertaining to synthesis of In₂Se₃ nanostructures employing a single step facile route (like thermal evaporation) are desirable; as such studies are scientifically as well as technologically meaningful and significantly contribute to the existing knowledge in this field. With the advent of nanotechnology, various researchers have reported synthesis and optoelectronic properties of different nano-forms of In₂Se₃, such as nanowires, nanotrees, nanobelts, and nanoflakes and its potential applications.¹⁻¹¹ In this regard, Q. L. Li *et al* have synthesized single crystalline In₂Se₃ nanowires array using horizontal tube furnace under controlled ambient of a mixture of Ar and H₂ gases at high temperature. The authors have explored the potential of nanowires as visible light photo-detector.¹² M. Lin *et al*. have reported an atomically thin epitaxial controlled growth of In₂Se₃ nanoflakes using horizontal tube furnace at high temperature.¹⁰ Recently, micromechanical exfoliation based synthesis of ultrathin single crystalline In₂Se₃ nanosheets has been attempted for extraordinary photo-detector applications.¹³ In spite of In₂Se₃ being a potential candidate for application in nano-optoelectronic devices, in particular as photo-detector, the literature survey reveals that reports on synthesis, temperature dependent growth mechanism and electrical characterization of different nanoform of In₂Se₃ nanostructures are sparse in contrast to other chalcogenides. So, there is scope to explore a facile synthesis route towards temperature dependent growth of In₂Se₃ nanostructures and its morphological dependent electrical characterization. Although synthesis of In₂Se₃ nanowires by thermal evaporation is attempted in horizontal tube furnace by evaporating pure In₂Se₃,

this synthesis protocol appears to be risky as handling of hydrogen gas at high temperature involves complication. The electrical characterization primarily in the context of cold cathode application necessitates nanostructure possessing high aspect ratio and moderate areal density, gives the wisdom to explore the basic underlying physics and possible technological applications.

Herein, we report synthesis, temperature and time dependent vapour phase growth of different In_2Se_3 nanoforms using a facile thermal evaporation route. Furthermore, morphology dependent field emission (FE) investigation of the as-synthesized In_2Se_3 nanostructures have been carried out, and observed to be superior to the other chalcogenides nanostructures.

2. Experimental Section

2.1 Synthesis of In_2Se_3 Nanowires

In the present investigations, single crystalline In_2Se_3 nanowires were synthesized using a facile thermal evaporation route. In a typical synthesis experiment, an alumina boat filled with an appropriate amount of mixture of high purity Indium (In) crystals and selenium (Se) powder was placed in middle of a programmable quartz tube furnace. A pre-cleaned Au coated Si substrate (Au thickness ~ 40 nm, 1.0 cm \times 1.0 cm) was placed on sample holder, which was kept at distance of 12 cm away from the alumina boat at distance of ~ 12 cm from the alumina boat at downstream of the inert gas flow. The quartz tube furnace was flushed with Argon (Ar), at a flow rate of 350 sccm for 3 hour. The furnace temperature, measured at the quartz tube center, was raised to 1000 $^\circ\text{C}$ at the rate of $10^\circ\text{C}/\text{min}$. During deposition of In_2Se_3 nanostructures, the Ar flow rate was maintained at 200 sccm. After two hours, the furnace was allowed to cool naturally under constant Ar flow. The Au/Si substrate was removed from the furnace, which showed presence of shiny blackish product uniformly covering the entire surface. This as-synthesized product was used for further characterization.

2.2 Characterizations

Scanning electron microscopy (SEM) (JEOL 6360A) was used to examine the surface morphology of the as-synthesized In_2Se_3 nanostructures and their elemental composition was obtained using Energy-Dispersive X-ray Spectrometer (EDAX). The structural analysis of the as-synthesized product was obtained by X-ray diffraction (XRD, D8 Advance, Bruker AXS). Furthermore, in-depth structural and morphological investigations were performed using transmission electron microscopy (TEM, Tecnai G^2 20 Twin, FEI). The optical properties were investigated using (UV-Visible-NIR spectrophotometer-Model-JASCO 670). The chemical compositional analysis of the as-synthesized In_2Se_3 nanostructures was carried out using X-ray photoelectron spectroscopy (XPS, VG Microtech ESCA 3000)

The field emission (FE) current density (J) versus applied electric field (E) and emission current (I) versus time (t) characteristics were measured in a planar 'diode' configuration at base pressure of $\sim 1.0 \times 10^{-8}$ mbar. A typical 'diode'

configuration consist of a phosphor coated indium tin oxide semitransparent glass plate (a circular disc having diameter ~ 40 mm) serve as an anode, and the In_2Se_3 nanostructures deposited on Au/Si wafers pasted on a stainless steel holder (diameter ~ 4.5 mm) serves as a cathode. The FE measurements were carried out at fixed cathode-anode separation of ~ 1 mm. The emission current was measured on Keithely Electrometer (6514) by sweeping dc voltage applied to cathode with a step of 40 V (0 - 40 kV, Spellman, U.S.). The UHV chamber is equipped with rotary backed turbo molecular pump, sputter ion pump and titanium sublimation pump. For achieving base pressure of $\sim 1 \times 10^{-8}$ mbar, the chamber is baked at 200°C for 24 hrs. Special care was taken to avoid any leakage current using shielded cables and ensuring proper grounding. Before recording the FE measurements, pre-conditioning of the cathode was carried out by keeping it at ~ 2000 volts for 30 min duration so as to remove loosely bound particles and/or contaminants by residual gas ion bombardment. In order to confirm the reproducibility and repeatability of the results, the FE measurements were performed on two samples synthesized under identical conditions.

3. RESULT AND DISCUSSION

3.1 XRD, SEM, and TEM investigations

A typical XRD spectrum of as-synthesized In_2Se_3 nanostructures (Figure 1) exhibits a set of well defined diffraction peaks implying crystalline nature of the specimen. These peaks are indexed to the hexagonal crystalline phase of In_2Se_3 with lattice parameter $a=7.11$, and $c=19.34$ nm (JCPDS card, No#71-0250). Interestingly the XRD pattern does not show diffraction peak(s) corresponding to other phases such as InSe, In_4Se_6 , In_2O_3 , etc. indicating high purity of the as-synthesized product. Thus, the XRD analysis clearly reveals formation of high purity crystalline In_2Se_3 phase under the prevailing experimental conditions. The scanning electron microscopy was used to reveal the surface morphology of the as-synthesized In_2Se_3 nanostructures on Au/Si wafer. Figures 2 (a-c) depict the SEM micrographs recorded at three different magnifications and show the formation of randomly distributed nanowires over the entire substrate surface. A cautious observation of the SEM images reveals the formation of ultra long nanowires having diameter in the range of ~ 50 to 70 nm. Figures 2 c & d exemplify that some of the nanowires are projecting away from the substrate surface. The EDAX spectrum (Figure 2 (d)) reveals presence of nearly stoichiometric ratio of In and Se in the as-synthesized product. The observation of very small quantity of oxygen in the EDAX spectrum may be attributed to incorporation of atmospheric oxygen in the sample, as it is exposed to ambient.

Furthermore, in depth structural analysis and understanding the crystallographic features of the as-synthesized product, TEM studies were carried out. Figure 3(a) depicts high magnification bright field TEM image, showing formation of In_2Se_3 nanowires, with diameters in the range of 50 - 70 nm complimenting to SEM results. The selected area electron diffraction (SAED) pattern, depicted in Figure 3(b) confirm the single crystalline hexagonal phase of the In_2Se_3 nanowires. The lattice-resolved HRTEM images of a single In_2Se_3 nanowire

(Figure 3(c, and d-digitally magnified)), confirm its crystalline nature. It exhibits two distinct fringe patterns with 'd' spacing of 1.40 and 0.35 nm corresponding to (1-120) and (1-100) planes of In_2Se_3 hexagonal phase, respectively.¹¹

3.2 Optical and X-ray photo-electron spectroscopy (XPS) analysis

To study the optical properties of the as-synthesized In_2Se_3 nanostructure, the UV-visible-NIR absorption spectrum was recorded in the range 900-1600 nm. The spectrum (Figure 4 a) exhibits high absorption in the short wavelength region, which decays rapidly with increase in the wavelength, showing negligible absorption in the long wavelength region. The inset of Figure 4 a depicts a plot of $(\alpha h\nu)^2$ versus photon energy ($h\nu$), known as a Tauc plot. The band gap energy, estimated from the Tauc plot, is found to be ~ 1.3 eV, which agrees well with the reported values.^{14,15,19}

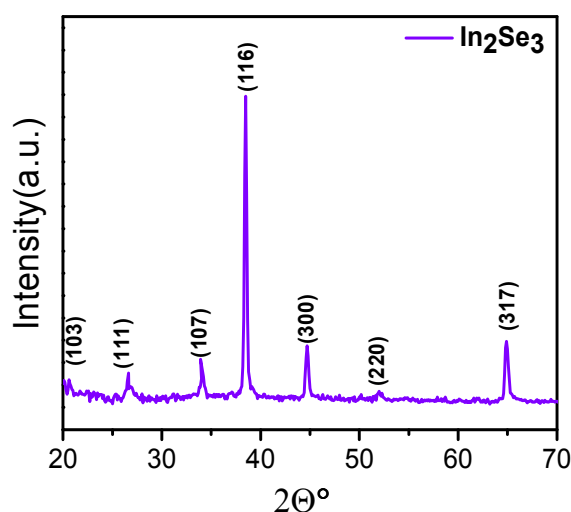


Fig. 1 A typical XRD pattern of the In_2Se_3 nanowires synthesized at distance ~ 12 cm from alumina boat.

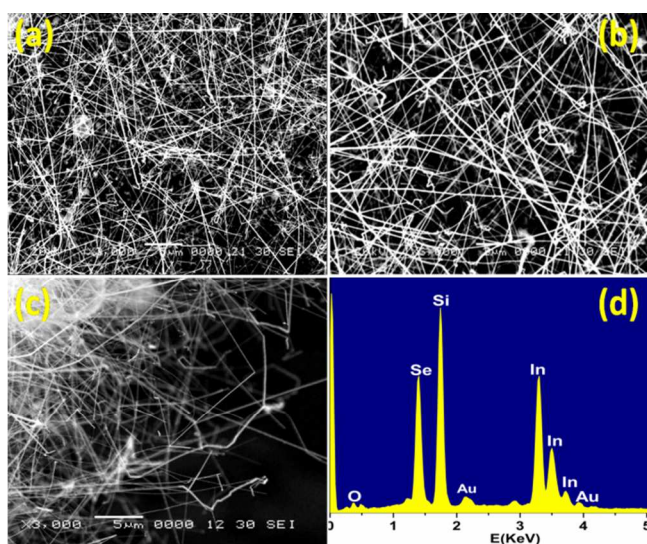


Fig. 2 SEM images of the In_2Se_3 nanowires deposited on Au/Si wafer recorded at different magnifications (a) 3,000x (b) 6,000x and (c) 3,000x showing some of the nanowires protruding away from the specimen edge (d) corresponding EDAX spectrum.

Figure 4 (b) depicts a survey scan of the XPS spectrum of as-synthesized In_2Se_3 nanowires. The XPS spectrum shows signatures of In and Se only, implying purity of the specimen.

The survey scan is further resolved in two different parts corresponding to In and Se energy states. Figure 4 (c) shows two strong peaks at 445.15 and 452.85 eV with splitting of 7.7 eV corresponding to In $3d_{5/2}$ and In $3d_{3/2}$, respectively, which is consistent with standard Indium. The observed In-3d spectrum is identical to those reported for various In_2Se_3 nanostructures and films.¹⁶⁻¹⁹ In addition to the In energy levels, a signature of Se3d level is observed at 54.9 eV (Figure 4(d)).

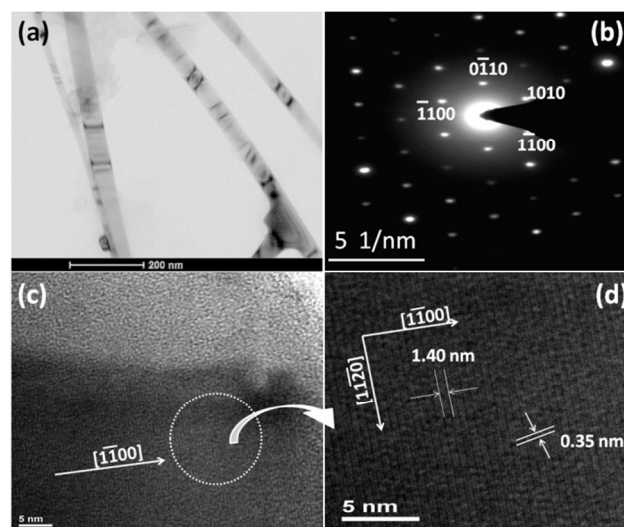


Fig. 3 TEM images of (a) the In_2Se_3 nanowires (b) selected area electron diffraction (SAED) pattern (c) high resolution TEM image of a single In_2Se_3 nanowires with magnified view in figure (d).

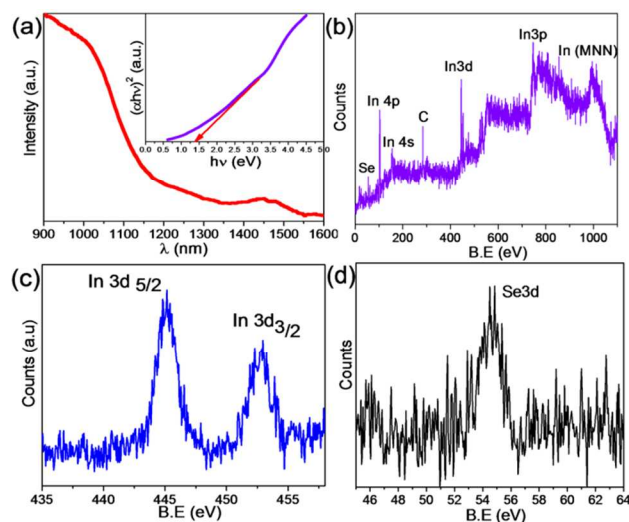
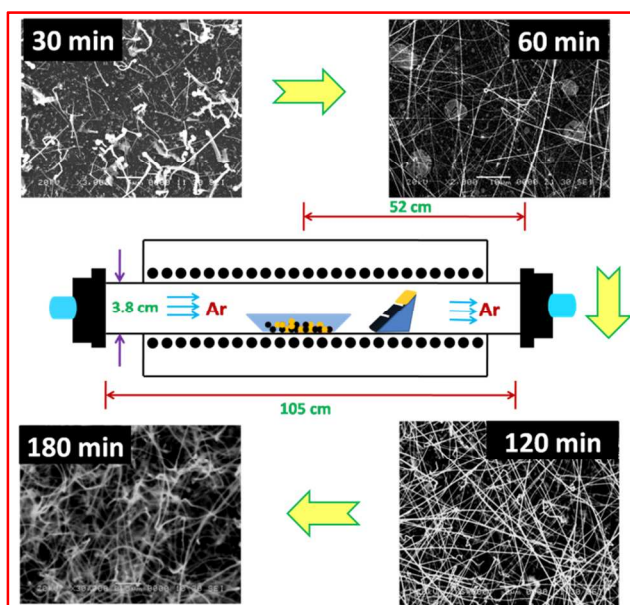


Fig. 4 (a) Optical absorption spectrum In_2Se_3 nanostructure with inset depicts a Tauc plot of $(h\nu)$ versus $(\alpha h\nu)^2$ derived from observed optical data (b) XPS Survey scan (c) In $3d_{5/2}$, Se $3d_{3/2}$ states (d) Se 3d state.

3.3 Time dependent morphological evolution

In order to reveal the effect of synthesis duration on the morphology and to elucidate the growth mechanism of In_2Se_3 nanostructures, several experiments were carried out by varying the synthesis time from 30 min to 180 min, keeping the other

process variables unchanged. Scheme: 1 depicts the SEM images of the In_2Se_3 nanostructures synthesized at different deposition periods. For 30 min deposition duration, formations of irregular nanostructures resembling to nanowires/rods possessing highly non uniform dimension is observed. When the deposition period were increased to 60 min, formation of less dense fine, long randomly distributed nanowires was observed, in addition to unreacted gold iceland seen in SEM image. For 120 min duration, the morphology of as-synthesized product is characterized by presence of very fine ultralong In_2Se_3 nanowires with moderate areal density.



Scheme 1: Schematic of time dependent morphological evolution of In_2Se_3 nanowires

Further increase in the deposition period to 180 min resulted in formation in bunching/clustering of nanowires. A careful observation of the SEM images reveal that the areal density of nanowires goes on increasing as deposition period increased and random network of the nanowires is observed at higher deposition duration.

3.4 Temperature Dependent Growth Mechanism

In order to shed more light on the growth mechanism of In_2Se_3 nanostructures, in another set of experiment, the synthesis was carried out by placing the substrates at different positions with respect to the source location. In the tubular furnace, there exists a temperature gradient along the tube length. We have measured the temperatures at different position in the quartz tube with respect to the source location and the temperature-position plot is depicted in figure 5. The synthesis was carried out by placing the substrates at 22, 20, 18, 16, 14, 12, 10, 7, 3 cm from the alumina boat and on its top. For systematic studies, only one substrate was kept at a time at a given position, following the synthesis protocol as mentioned earlier. Based on the XRD and SEM analysis, we herein propose a plausible growth mechanism of the In_2Se_3 nanostructures, depicted in Scheme: 2.

The pristine Au/Si substrate exhibits grainy, coarse morphology uniformly covering the entire substrate surface. When the

deposition was carried out by keeping the substrate at 22 cm, highly non-uniform deposition of Au-In phase was observed. The formation of Au-In eutectic phase has been confirmed from the XRD analysis, however for the sake of brevity the XRD pattern is not shown here. The overall morphology of the deposit is characterized by presence of randomly distributed, irregular shaped Au-In islands. A careful observation of the SEM image reveals presence of un-reacted Au nanoparticles on the substrate surface. From the temperature calibration plot, the substrate temperature at this position is estimated to be 680 °C. As seen from the phase diagram of In-Se binary alloy, at this temperature the alloy exhibits 'peritectic' phase of In-Se. Similarly, from the phase diagram of Au-In binary alloy, this temperature corresponds to presence Au-In eutectic phase.²⁰ Thus, the XRD analysis revealing formation of only Au-In eutectic phase, and not showing signatures of In_2Se_3 phase, is in agreement with phase diagrams of both the alloys. At 20 and 18 cm positions, corresponding to temperatures of 745 and 780 °C respectively, the XRD spectra showed low intensity signature(s) of In_2Se_3 phase, in addition to the Au-In phase. The corresponding SEM images (Figs. (b) and (c), Scheme: 2) reveal gradual change in morphology characterized by presence of uniformly distributed grains (might be of In_2Se_3 phase) at 780 °C. The formation of In_2Se_3 phase at these temperatures is in agreement with its phase diagram.²⁰ As with further decrease in the distance of substrate position, i.e. keeping the substrates at 16, 14, 12 cm, the XRD spectra exhibit weakening of the Au-In phase signatures with simultaneous increase in intensity of the diffraction peaks due to In_2Se_3 phase. The corresponding SEM images (Figs. (d-g), Scheme: 2) interestingly show transformation from granular structures to one-dimensional nanostructures, with increase in the temperature. At substrate temperature of 870 °C (substrate position ~ 12 cm), formation of very fine ultra long In_2Se_3 nanowires is observed (Fig. (g), Scheme: 2). When the substrates were kept at 10, 07 and 05 cm away from the source, the corresponding SEM images shows variation in the morphology of the In_2Se_3 nanostructure. It indicates that, irrespective of the deposition duration, at higher substrate temperature more than 870 °C, the In_2Se_3 nanowires start clustering together. The length of the nanostructures exhibits significant reduction in their length with increase in the base diameters and at substrate position of 10 cm (temperature ~920 °C) formation of nano-whisker/rods was observed (Fig. (h), Scheme: 2). subsequently at higher temperature (substrate position 07 cm) formation of micron sized clusters is observed (Fig. (i), Scheme: 2). Interestingly, with further increase in temperature, (substrate position 05, and 03 cm) formation of non-uniform, randomly distributed granular structures is observed, which could be due to unfavorable thermodynamic conditions (Fig. (j), and (k), Scheme: 2). Finally, when the substrate was kept on top of the alumina boat, formation of spherical In_2Se_3 particles with less areal density is observed (Fig. (l), Scheme: 2). A careful observation of the SEM images (Figs. (j-l), Scheme: 2) reveals that the area density of In_2Se_3 structures is decreasing as the substrate temperature is increased beyond 920 °C. The variation in phase and morphology of the resultant product(s) obtained on the substrate surface as a function of its position from the source can be exemplified with

the help of phase diagrams and thermodynamic conditions including, substrate temperature, vapour pressure of the source and collector phase (condensate on the substrate). Furthermore, the kinematics of various processes like adsorption, absorption, diffusion, condensation and vaporization, etc needs to be considered to understand the growth mechanism and resultant morphology. We believe that the growth of In_2Se_3 nanostructures is as per the VLS mechanism, wherein the gold layer on the substrate plays catalytic role. With the help of phase diagram, one can predict the behaviour of a catalyst in these processes/interactions. ^{8, 11, 21, 22} C. C. Lee *et al* have exemplified the temperature dependent change in the chemical composition of Au-In eutectic alloy using its binary phase diagram.²⁰ With increase in the temperature of the supply phase, its vapourization rate increases. At the collector phase, more quantity of eutectic alloy is formed, in the same deposition period. The quantitative change in the eutectic phase concentration at different temperatures leads to variation in the surface morphology.

In the present studies, at each substrate position (and corresponding temperatures) formation of the Au-In droplets is thermodynamically anticipated, since the respective substrate temperatures are higher than the eutectic phase temperature of Au-In phase, 454 °C. As the furnace temperature is raised, initially the Au film exhibits thermally activated transformation leading to formation of Au-In nano-droplets. These Au-In nano-droplets act as energetically favoured sites for adsorption of the incoming In and Se vapours drifted by the carrier (Ar) gas species. With gradual absorption and/or diffusion of the In and Se atomic species onto the interface between the supply and collector phase, the liquid droplets reach supersaturation and growth of stable In-Se phase is initiated via vapour-liquid-solid (VLS) mechanism. From the phase diagram of binary In-Se alloy, it is observed that the In_2Se_3 phase (polymorphic) exists at temperature ~ 730 °C and above, implying minimum substrate temperature of this value (substrate positions less than 18 cm) for formation stable In_2Se_3 phase. Thus the observation of small micron size crystallites of In_2Se_3 observed on substrate kept at 16 cm is thermodynamically justified. Subsequently at higher substrate temperature of ~850 °C, formation of one-dimensional (1-D) In_2Se_3 nanostructures is observed. Such morphological transformation during VLS mechanism has been observed by many researchers for various semiconducting nanostructures like SnS, GaS, ZnS etc.^{1, 23, 24}, which is primarily due to migration of the catalytic particles along the vertical direction rather than in lateral directions, as the growth progresses. The 1D growth is mainly due to direct incorporation of the vapour species than the contribution from species due to the surface diffusion. It is well known that in case of VLS growth, many a times, presence of the catalyst particle is observed at the tip of the 1D nanostructures. In our case too, the insets of Figures (e, and f), Scheme: 2 show presence of Au-In droplet at the tip of the In_2Se_3 nanowires. Owing to their high secondary electron emission yield; the Au-In nuclei appear 'bright' in contrast to the In_2Se_3 counterpart.

With further increase in the temperature, (~870 °C), the length of the In_2Se_3 nanowire increases with simultaneous reduction in its diameters. At the substrate position ~ 12 cm, formation of ultra long and extremely fine In_2Se_3 nanowires is observed.

Interestingly, in case of these ultra long In_2Se_3 nanowires, presence of Au-In nuclei at the tip of nanowires is not observed in the SEM image. It is expected that, due to ultra long nature of the nanowires the Au-In particles might have detached from the tip of the nanowires at some point of growth.

At these substrate positions, the corresponding temperatures being higher, thermally activated diffusion rate of adsorbed vapour species increases leading to more/faster growth along the lateral directions than the vertical one. Thus the observation of 'granular' morphology, instead of well defined 1D nanostructures at higher substrate temperature can be expected as per the Ostwald ripening occurs between nanoparticles.

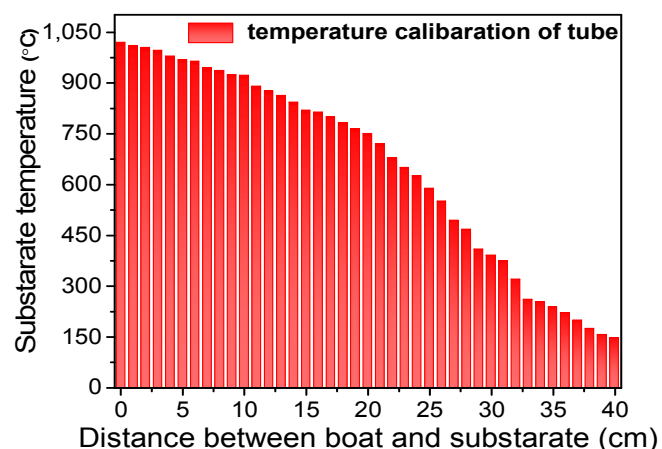
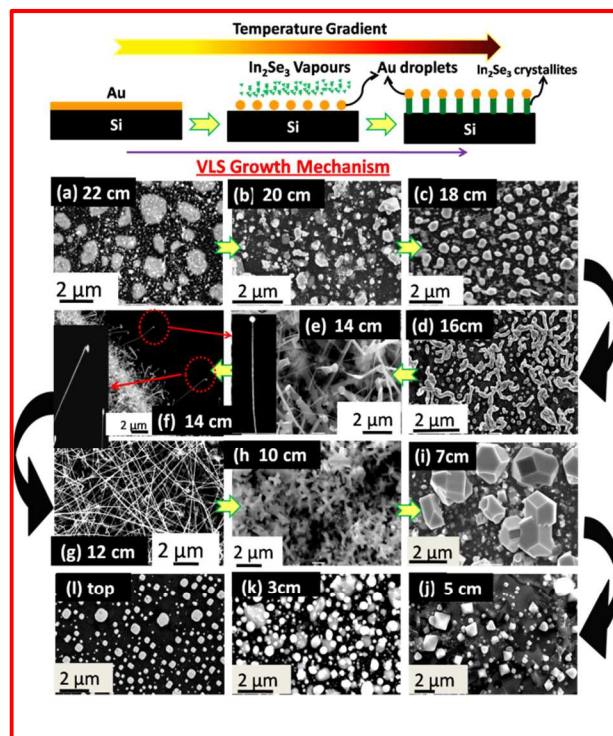


Fig. 5 Temperature calibration plot of the horizontal tube furnace.



Scheme 2: Schematic VLS growth mechanism of In_2Se_3 nanostructure.

Ostwald ripening is a spontaneous process that occurs because larger particles are more energetically favourable. Accordingly, nanoparticles tend to transform into large particles to attain a lower energy state. Onto the top position of alumina boat substrate temperature was so higher ~ 1000 °C which directly melts the gold on substrate surface.^{1, 23-26}

In general, the growth characteristics and properties of the nanowires is found to be catalyst dependent. The diameter of the Au-In droplet is one of the crucial parameters governing the overall growth of the nanostructures.^{1, 23-26} Measurements over a large number of nanowires have revealed that when the diameter of the droplet is equal to or smaller than the width of the nanowires, no bending occurs and straight nanowires are developed, whereas in case of large size droplets, the nanowires exhibit tendency to change the growth direction at an angle with respect to the initial growth axis. In the present investigation, we have observed formation of a few "L" shaped nanowires as shown in scheme: 2 inset figure e & f.

The rate of diffusion of the vapour and/or adsorbed species across the interfaces like gas/solid, gas/liquid, and liquid/solid) is an important parameter describing the VLS mechanism. The kinetics of the VLS mechanism consists of four steps: (1) mass transport in the gas phase; (2) chemical reaction at the vapour-liquid interface; (3) diffusion in the liquid phase; and (4) incorporation of atoms in a crystal lattice. To draw some insight based on the experimental results and literature reports, the rate-determining step for the growth of 1D In₂Se₃ structures could be claimed as follows: Among the above steps, the step (3) can be excluded, because atoms diffuse in liquid metals very quickly and thick nanowires or whiskers grow rapidly than the thinner ones. In addition, the shape of the liquid droplet is maintained nearly hemispherical and retains a longer diffusion length. The step (1) can also be excluded because the diffusion coefficient in the gaseous phase usually follows the following power law as follows,^{1, 23-26}

$$D = D_0 \left(\frac{T}{T_0}\right)^n \left(\frac{P}{P_0}\right) \quad n=1.5-2 \quad (1)$$

Therefore, the growth rate should follow the power law. Where, D, T, P are the diffusion, temperature and pressure coefficients. From the growth kinetics point of view, the VLS mechanism laid prominence on surface adsorption/diffusion of reactant species/atoms/molecules/ions and their preferential/favoured incorporation at high-surface-energy facets/sites sustained the uninterrupted growth of nanostructures. The process can elucidate the intrinsic crystallography of materials into nanostructures to form well-faceted structures. In-Se being a layered structure, during its growth it has many dangling bonds at the two edges, which can easily incorporate atoms directly from the vapour phase or diffusing from the bottom surface. So, some contribution of the vapour-solid (VS) growth can be anticipated, in addition to the VLS process.^{1, 23-26} The low vapour pressure (order of 10^{-7} bar at 12 cm deposition position), and low ionic mobility of In, ensures a sluggish and steady supply of source metal species/atoms/molecules/ions that may favour growth of such fine nanostructures.

3.5 Field Emission

The field emission current density versus applied field (J-E) characteristic of the In₂Se₃ nanostructures is depicted in Figure 6(a). The values of the turn-on and threshold field, defined as field required to draw an emission current density 1 and 10 $\mu\text{A}/\text{cm}^2$, respectively observed for the In₂Se₃ nanostructures are listed in Table-1. Interestingly, high emission current density of ~ 1.220 mA/cm² has been drawn from the In₂Se₃ nanowires emitter at relatively lower applied electric field of ~ 6.33 V/ μm . For sake of comparison, Table-2 presents compilation of morphology, turn on and threshold field values of different material chalcogenide nanostructures and nanocomposite emitters. The observed turn-on field, threshold field, field enhancement factor and emission current density are observed to be strongly influenced by morphology (aspect ratio) of In₂Se₃ nanostructures. Among all nanostructures, the lowest values of the turn-on and threshold field are observed for the In₂Se₃ nanowires emitter, which is attributed to the high aspect ratio of the nanowires owing to their very fine diameter and ultra long nature. Furthermore, as seen from the SEM images, the areal density of the In₂Se₃ nanowires is seen to be moderate, offering less field screening effect. Thus, the observed superior values of turn-on and threshold field, and extraction of high emission current density at lower applied electric field is attributed synergic effect of high aspect ratio, smaller areal density, less screening effect of the In₂Se₃ nanowires.

The field emission characteristics were further analyzed by modified form of Fowler-Nordheim equation for multi-tip assembly, which is given by,^{32,33}

$$J = \lambda_M a \phi^{-1} E^2 \beta^2 \exp\left(-\frac{b\phi^3}{\beta E} \nu_F\right) \quad (2)$$

where J is the emission current density, E is the applied average electric field, a and b are constants, typically 1.54×10^{-10} (AV⁻²eV) and 6.83×10^3 (VeV^{-3/2} μm^{-1}), respectively, ϕ is the work function of the emitter material (~ 4.50 eV), λ_m is a macroscopic pre-exponential correction factor, ν_F is value of the principal Schottky-Nordheim barrier function (a correction factor), and β is the field enhancement factor.

Table No. 1: Comparison of synthesis route, field emission turn-on and threshold value of different materials.

Sr. No.	Morphology	Synthesis route	Turn-on field(V/ μm)	Threshold field (V/ μm)	Reference
1	Bi ₂ S ₃ nanowires	Hydrothermal synthesis	0.1 $\mu\text{A}/\text{cm}^2$ at 2.08	50 $\mu\text{A}/\text{cm}^2$ at 3.36	28
2	GaS nanobelts	Thermal evaporation	0.1 nA/cm ² at 2.9	5.7 $\mu\text{A}/\text{cm}^2$ at 6.0	23
3	ZnS nanotubes	Controlled evaporation	10 $\mu\text{A}/\text{cm}^2$ at 3.47	11.5 mA/cm ² at 5.5	29
4	WS ₂ nanosheets	Hydrothermal synthesis	1 $\mu\text{A}/\text{cm}^2$ at 4.10 V/ μm	10 $\mu\text{A}/\text{cm}^2$ at 5.0	30
5	SnS nanowires	Thermal evaporation	1 $\mu\text{A}/\text{cm}^2$ at 1.65 V/ μm	10 $\mu\text{A}/\text{cm}^2$ at 1.98	1
6	Ag-rGO composite	Chemical reflux route	1 $\mu\text{A}/\text{cm}^2$ at 2.40 V/ μm	10 $\mu\text{A}/\text{cm}^2$ at 2.80	31
7	In ₂ Se ₃ nanowires	Thermal evaporation	1 $\mu\text{A}/\text{cm}^2$ at 3.40 V/ μm	10 $\mu\text{A}/\text{cm}^2$ at 4.17	Present work

The Fowler-Nordheim (F-N) plot derived from the observed J-E

characteristic is shown in Figure 6 (b). The F-N plot shows a non-linear nature. Furthermore, the emission current density J is estimated as $J = I/A$, where, I is the observed value of emission current and A is the total area of the emitter ($\sim 1 \text{ cm}^2$). As a result, the estimated value of field enhancement factor (β) for In_2Se_3 nanowires is ~ 3596 and consequently get decreased as the aspect ratio decreases of different In_2Se_3 nanostructure.

The emission current *versus* time (I-t) plot corresponding to preset value of $\sim 1 \mu\text{A}$, recorded over a period of more than 3 hours at a base pressure of 1×10^{-8} mbar, is depicted in Figure 6 (c). The emission current is seen to remain extremely stable over the entire duration, which indicates no degradation of the emitter with good physical and chemical stability of the emitter. The emission current stability of a planar emitter is governed by extrinsic parameters such as areal density, shape and size distribution of the nanostructures, in addition to the intrinsic properties of the emitter material like electrical conductivity, chemical inertness, mechanical robustness against ion bombardment and field induced stresses. In the present case the good emission stability exhibited by the In_2Se_3 nanowires emitter can be attributed to uniform size distribution of the nanowires and their moderate areal density. Furthermore, the pre-conditioning carried out by keeping the emitter at 2000 volts for 30 minutes duration may have cleaned the emitter. Also during long term stability the in-situ cleaning due to continuous ion bombardment cleaning of the emitter surface assist in stabilizing the emission current. Figure 6 (d) shows the field emission image indicates of bright shiny spots, confirming that the emission is indeed from the most protruding In_2Se_3 nanowires. The overall superior field emission characteristics demonstrate the In_2Se_3 nanowires field emitter as a potential candidate in electron source for practical applications in various vacuum micro-nano electronic devices.

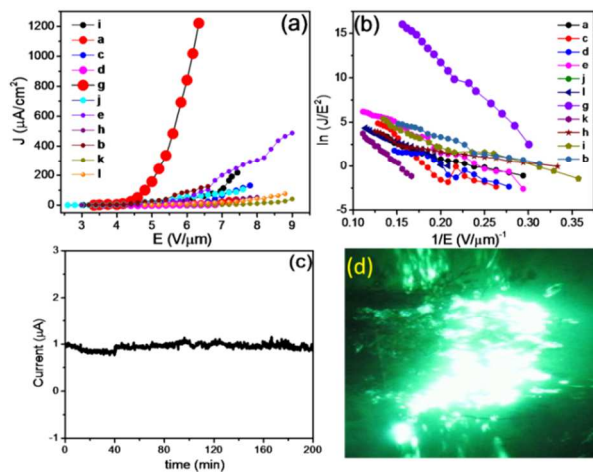


Figure 6 (a) The field emission current density versus applied electric field (J-E) curve of In_2Se_3 NWs (b) F-N plot (c) The emission current versus time (I-t) plot of In_2Se_3 NWs (d) shows field emission micrograph.

Table No. 2: Comparison of field emission turn-on and threshold value of different nanostructure In_2Se_3

Sample No.	Turn-on field (V/ μm) at $\sim 1 \mu\text{A}/\text{cm}^2$	Threshold field (V/ μm) at $\sim 10 \mu\text{A}/\text{cm}^2$	Maximum current density ($\mu\text{A}/\text{cm}^2$) at V/ μm	Field enhancement factor (β)	
a	~ 4.40 V/ μm	~ 6.50 V/ μm	$\sim 32 \mu\text{A}/\text{cm}^2$ at ~ 7.40 V/ μm	2341	
b	~ 3.20 V/ μm	~ 4.40 V/ μm	$\sim 125 \mu\text{A}/\text{cm}^2$ at ~ 6.60 V/ μm	2109	
c	~ 5.60 V/ μm	~ 6.20 V/ μm	$\sim 132 \mu\text{A}/\text{cm}^2$ at ~ 7.80 V/ μm	1109	
d	~ 5.00 V/ μm	~ 6.80 V/ μm	$\sim 6 \mu\text{A}/\text{cm}^2$ at ~ 6.80 V/ μm	1873	
e	~ 4.20 V/ μm	~ 5.25 V/ μm	$\sim 480 \mu\text{A}/\text{cm}^2$ at ~ 9.00 V/ μm	1368	
g	~ 3.40 V/ μm	~ 4.17 V/ μm	$\sim 1.2 \text{ mA}/\text{cm}^2$ at ~ 6.33 V/ μm	3596	
h		~ 3.20 V/ μm	~ 6.40 V/ μm	$\sim 53 \mu\text{A}/\text{cm}^2$ at ~ 8.00 V/ μm	582
i		~ 3.42 V/ μm	~ 5.30 V/ μm	$\sim 218 \mu\text{A}/\text{cm}^2$ at ~ 7.44 V/ μm	2304
j	~ 3.60 V/ μm	~ 4.50 V/ μm	$\sim 106 \mu\text{A}/\text{cm}^2$ at ~ 7.60 V/ μm	758	
k	~ 3.30 V/ μm	~ 5.00 V/ μm	$\sim 75 \mu\text{A}/\text{cm}^2$ at ~ 8.80 V/ μm	755	
l	~ 6.60 V/ μm	~ 8.00 V/ μm	$\sim 42 \mu\text{A}/\text{cm}^2$ at ~ 9.00 V/ μm	1568	

4. CONCLUSION

In conclusion, synthesis of single crystalline In_2Se_3 nanowires on Au/Si substrate has been accomplished by a facile thermal evaporation technique under optimized process variables. The XRD and XPS analysis reveals the formation of pure hexagonal phase of In_2Se_3 under the optimized conditions. The FE characteristics of the In_2Se_3 nanowires emitter in terms of turn-on and threshold field values are found to be superior to those reported for other chalcogenides nanostructures. The In_2Se_3 nanowires emitter exhibits extremely stable emission at preset value of $\sim 1 \mu\text{A}$ over long term duration of more than 3 hours.

Acknowledgments

Mr. Sachin Suryawanshi gratefully acknowledges the financial support from BARC, Mumbai, for the award of Senior Research Fellowship under BARC-UoP memorandum (Grant code: GOI-E-153). Prof. M. A. More would like to thank the BCUD, University of Pune for the financial support provided for the field emission work under CNQS-UPE-UGC program activity. Dr. D. J. Late would like to thank Prof. C. N. R. Rao (FRS), JNCASR and ICMS Bangalore (India) for encouragement, support and the experimental facilities. The research work was supported by Department of Science and Technology (Government of India) under Ramanujan Fellowship (Grant No.

SR/S2/RJN-130/2012), NCL-MLP project grant 028626, DST-SERB Fast-track Young scientist project Grant No. SB/FT/CS-116/2013, Broad of Research in Nuclear Sciences (BRNS) (Government of India), partial support by INUP IITB project sponsored by DeitY, MCIT, Government of India and CINT Proposal #U2015A0083 (USA).

¹Department of Physics, Savitribai Phule Pune University Pune-411007, Maharashtra, India

²Physical & Materials Chemistry Division, CSIR-National Chemical Laboratory, Dr. Homi Bhabha Road, Pune 411008, Maharashtra, India datta099@gmail.com / dj.late@ncl.res.in, mam@physics.unipune.ac.in.

Notes and references

1. S. R. Suryawanshi,; S. S. Warule,; S. S. Patil,; K. R. Patil,; M. A. More, *ACS Appl Mater Interfaces* 2014, **6**, 2018-25.
2. A. Datta,; P. G. Chavan,; F. J. Sheini,; M. A. More,; D. S. Joag, A. Patra, *Crystal Growth & Design* 2009, **9**, 4157-4162.
3. K. Winkler, E. Bertagnolli, A. Lugstein, *Nano Lett.* 2015, **15**, 1780-5.
4. D. Kang,; T. Rim,; C. k. Baek,; M. Meyyappan,; J. S. Lee., *Small* **2014**, *10* 18, 3795-802.
5. Y. Zou, Z. G. Chen,; Y. Huang,; L. Yang,; J. Drennan,; J. Zou, *J. Phys. Chem. C* 2014, **118**, 20620-20626.
6. Li, D.; Zhang, J.; Wang, X.; Huang, B.; Xiong, Q., *Nano Lett.* 2014, **14**, 4724-8.
7. T. Zhai, X. Fang,; M. Liao; X. Xu; L. Li,; B. Liu; Y. Koide, Y. Ma,; J. Yao,; Y. Bando, D. Golberg, *ACS Nano* 2010, **4**, 1596-602.
8. X. Sun, B. Yu, G. Ng,; T. D. Nguyen,; M. Meyyappan, *Appl. Phys. Lett.* 2006, **89**, 233121.
9. Y. Zou, Z. G. Chen,; Y. Huang,; L. Yang,; J. Drennan,; J. Zou., *J. Phys Chem. C* 2014, **111**, 20620-20626.
10. M. Lin; D. Wu; Y. Zhou; W. Huang; W. Jiang, W. Zheng, S. Zhao,; C. Jin, Y. Guo; H. Peng, Z. Liu, *J Am Chem Soc* 2013, **135**, 13274-7.
11. H. Peng ,D. T. Schoen; S. Meister, X. F. Zhang,; Y. Cui, *J Am Chem. Soc.* 2007, **129**, 34-39.
12. Q. L. Li; Y. Li; J. Gao; S. D. Wang; X. H. Sun, *Appl. Phy. Lett.* **2011**, *99* 24, 243105.
13. R. B. Jacobs-Gedrim; M. Shanmugam; N. Jain, C. A. Durcan,; M. T. Murphy; T. M. Murray, R. J. Matyi; Moore, R. L., 2nd; Yu, B., *ACS Nano* 2014, **8**, 514-21.
14. In₂Se₃ band structure, energy gaps. In *Ternary Compounds, Organic Semiconductors*, Madelung, O.; Rössler, U.; Schulz, M., Eds. Springer Berlin Heidelberg: **2000**; Vol. 41E, pp 1-5.
15. C. Julien, A. Chevy; D. Siapkas, *Physica Status Solidi (a)* 1990, **118**, 553-559.
16. B. Thomas, *Appl. Phys. A* **1992**, *54* 3, 293-299.
17. P. Liu, S. Yu, W. Fan; W. Shi, *Dalton Trans* 2013, **42**, 2887-93.
18. H. E, Maliki,; S. Marsillac,; J. C. Bernède; E. Faulques; J. Wery, *J. of Phy.: Cond. Matter* 2001, **13**, 1839-1850.
19. M. Emziane; Ny, R. L., *J. Phy. D: Appl. Phy.* 1999, **32**, 1319-1328.
20. T. B. Massalski *Binary Alloy Phase Diagrams, ASM International; 2nd Revised edition edition (15 July 1990) ISBN-10: 087170403X, ISBN-13: 978-0871704030*

21. C. C. Lee, C. Y. Wang; G. Matijasevic, *IEEE Transactions on Components, Hybrids, and Manufacturing Technology* 1993, **16**, 311-316.
22. R. W. Cahn, *Binary Alloy Phase Diagrams-Second edition*. T. B. Massalski, Editor-in-Chief; H. Okamoto, P. R. Subramanian, L. Kacprzak, Editors. ASM International, Materials Park, Ohio, USA. December 1990.
23. S. K. Panda; A. Datta; G. Sinha; S. Chaudhuri, P. G. Chavan,; S. S. Patil; M. A. More; D. S. Joag, *J. Phys. Chem. C* 2008, **112**, 6240-6244.
24. X. Wang; C. J. Summers,; Z. L. Wang, *Nano Lett* 2004, **4**, 423-6.
25. B. A. Wacaser,; K. A. Dick,; J. Johansson, M. T. Borgström,; K. Deppert,; L. Samuelson, *Adv. Mater.* 2009, **21**, 153-165.
26. H. J. Choi,; In *Semiconductor Nanostructures for Optoelectronic Devices*, Yi, G.-C., Ed. Springer Berlin Heidelberg: 2012; pp 1-36.
27. F. Geiger; C. A. Busse; R. I. Loehrke, *Inter. J Thermophy.* 1987, **8**, 425-436.
28. S. S. Warule; N. S. Chaudhari; B.B. Kale; S. Pandiraj; R. T. Khare,; M. A. More, *Cryst Eng Comm* , 2013, **15**, 890- 896.
29. X. S. Fang, ; Y. Bando, G. Z. Shen, C. H. Ye, U. K. Gautam, P. M. Costa, F. J.; Zhi, C. Y.; C. C. Tang,; D. Golberg, *Adv. Mater.* 2007, **19**, 2593-2596.
30. S. R. Suryawanshi, P. S. Kolhe, C. S. Rout, D. J. Late and M. A. More, *Ultramicroscopy*, 2015, **149**, 51-57.
31. A. K. Samantara, D. K. Mishra, S. R. Suryawanshi, M. A. More, R. Thapa, D. J. Late, B. K. Jena and C. S. Rout, *RSC Adv.* **5** (52), 41887-41893 (2015).
33. R. H. Fowler; L. Nordheim., *Proc. of the Ro. Soc. of London. Sr. A, Containing Papers of a Math. and Phy. Character* 1928, **119**, 173.
33. R. G. Forbes., *Nanotech.* 2012, **23**, 095706.